Journal of Catalysis 320 (2014) 70–76

Contents lists available at ScienceDirect

Journal of Catalysis

journal homepage: www.elsevier.com/locate/jcat

Imidazolium-based organoiridium-functionalized periodic mesoporous organosilica boosts enantioselective reduction of α-cyanoacetophenones, α-nitroacetophenones, and β-ketoesters

Boxin Deng, Wei Xiao, Cuibao Li, Feng Zhou, Xuelin Xia, Tanyu Cheng, Guohua Liu *

Key Laboratory of Resource Chemistry of Ministry of Education, Shanghai Key Laboratory of Rare Earth Functional Materials, Shanghai Normal University, Shanghai 200234, PR China

ARTICLE INFO

Article history:
Received 4 May 2014
Revised 22 September 2014
Accepted 28 September 2014

Keywords:
Asymmetric catalysis
Heterogeneous catalysis
Immobilization
Mesoporous materials
Silica

ABSTRACT

An imidazolium-based, organoiridium-functionalized periodic mesoporous organosilica is developed through complexation of chiral pentafluorophenylsulfonyl-1,2-diphenylethylenediamine and organoiridium-functionalized periodic mesoporous organosilica. Structural analyses and characterizations of catalyst reveal well-defined single-site iridium active species within its organosilicate network. Electron microscopy confirms a highly ordered dimensional-hexagonal mesostructure. This bifunctional heterogeneous catalyst displays excellent catalytic performance in the enantioselective reduction of α-cyano and α-nitroacetophenones. As expected, incorporation of imidazolium-functionality within hydrophobic periodic mesoporous organosilica promotes catalytic activity and enantioselectivity. In addition, this heterogeneous catalyst can be recovered and reused for at least eight times without loss of its catalytic activity. Furthermore, the approach described here can also construct another organoiridium-functionalized periodic mesoporous organosilica through postcoordination of chiral methylsulfonyl-1,2-diphenylethylenediamine, which provides excellent catalytic activity and enantioselectivity in the enantioselective reduction of β-ketoesters. The method presented here offers a potential way for immobilizing various chiral ligands to construct chiral organometal-functionalized periodic mesoporous organosilicas.

1. Introduction

Development of periodic mesoporous organosilicas (PMO) supports to immobilize various chiral organometallic complexes for asymmetric catalysis has attracted much interest [1,2]. Similar to inorganosilica mesoporous materials such as SBA-15 and MCM-41 [3,4], PMOs also possess large specific surface area and pore volume, tunable pore dimension, well-defined pore arrangement, as well as high thermal and mechanical stability. But in contrast to inorganosilicate mesoporous materials, PMOs have high hydrophobicity due to their intrinsic organosilicate inner surface, a significant advantage as it greatly promotes organic transformation [5,6]. Moreover, a PMO with imidazolium functionality in its organosilicate network can synergistically facilitate an organic reaction in a biphase catalytic system [7–9]. Although many achiral PMOs, including some imidazolium-based PMOs, have been reported [10–13], incorporation of the imidazolium functionality in a chiral ligand- or organometal-functionalized PMO network for asymmetric catalysis is still rare. Furthermore, general strategy for constructing PMO through assembly often requires a chiral ligand-derived silane [14–17]. However, the complicated synthetic process and tedious purification steps still limit their practical applications; chiral ligand-derived silanes are difficult to purify by silica gel column chromatography. Thus, utilizing the approach of direct postcoordination of chiral ligands may be a worthwhile alternative for constructing chiral organometal-functionalized PMOs, which has not been exported yet.

In our effort to develop various heterogeneous catalysts based on mesoporous silica [18–24], we found that several chiral organometal-functionalized PMOs have high hydrophobicity and could greatly promote asymmetric reactions [18,19]. We also found that the imidazolium-functionality within an organic–inorganic hybrid silica could significantly enhance the performance of a biphase catalytic reaction [20–22]. In the present contribution, we assembled a hydrophobic, imidazolium-based PMO by incorporating an imidazolium functionality in an ethylene-bridged PMO. Taking advantage of the postcoordination of (*S*,*S*)-pentafluorophenylsulfonyl-1,2-diphenylethylenediamine (PFPSDPEN), we developed a hydrophobic, imidazolium-based, organoiridium-functionalized heterogeneous catalyst. This catalyst efficiently facilitated the enantioselective reduction of α-cyanoacetophenones and

* Corresponding author. Fax: +86 21 64321819.
E-mail address: ghliu@shnu.edu.cn (G. Liu).

http://dx.doi.org/10.1016/j.jcat.2014.09.019
0021-9517/

α-nitroacetophenones in aqueous medium. As expected, the salient imidazolium-functionality and the high hydrophobicity of the PMO synergistically boosted the catalytic performance in aqueous medium. In addition, the heterogeneous catalyst could be recovered and reused for at least eight times without loss of its catalytic activity. Furthermore, applying the approach of direct postcoordination of chiral ligands, we also constructed another chiral organoiridium-functionalized heterogeneous catalyst through postcoordination of (*S*,*S*)-methylsulfonyl-1,2-diphenylethylenediamine and imidazolium-based PMO, which efficiently catalyzed the highly enantioselective reduction of β-ketoesters in aqueous medium.

2. Experimental

2.1. Characterization

Ir loading amount in the catalyst was analyzed using an inductively coupled plasma optical emission spectrometer (ICP, Varian VISTA-MPX). Fourier transform infrared (FT-IR) spectra were collected on a Nicolet Magna 550 spectrometer using KBr method. X-ray powder diffraction (XRD) was carried out on a Rigaku D/Max-RB diffractometer with Cu Kα radiation. Scanning electron microscopy (SEM) images were obtained using a JEOL JSM-6380LV microscope operating at 20 kV. Transmission electron microscopy (TEM) images were performed on a JEOL JEM2010 electron microscope at an acceleration voltage of 220 kV. X-ray photoelectron spectroscopy (XPS) measurements were taken on a Perkin-Elmer PHI 5000C ESCA system. A 200 μm diameter spot size was scanned using a monochromatized Aluminum Kα X-ray source (1486.6.6 eV) at 40 W and 15 kV with 58.7 eV pass energies. All the binding energies were calibrated by using the contaminant carbon (C_{1s} = 284.6 eV) as a reference. Nitrogen adsorption isotherms were measured at 77 K with a Quantachrome Nova 4000 analyzer. The samples were measured after being outgassed at 423 K overnight. Pore size distributions were calculated by using the BJH model. The specific surface areas (*S*BET) of samples were determined from the linear parts of BET plots (p/p_0 = 0.05–1.00). Thermal gravimetric analysis (TGA) was performed with a Perkin-Elmer Pyris Diamond TG analyzer under air atmosphere with a heating ramp of 5 K/min. Solid-state ^{13}C (100.5 MHz) and ^{29}Si (79.4 MHz) CP MAS NMR were obtained on a Bruker DRX-400 spectrometer (CP times: 2 ms, spinning speed 5 KHz, pulse lengths: 4 μs). Elemental analysis was performed with a Carlo Erba 1106 Elemental Analyzer.

2.2. Catalyst preparation

2.2.1. Preparation of HO_3S-PMO (**3**)

In a typical synthesis, 2.0 g of structure-directing agent, pluronic P123, was completely dissolved in a mixture of 80 mL of hydrochloric acid (0.2 N) and 6.0 g of KCl. The mixture was stirred at room temperature for 1.0 h. Subsequently, 3.22 g (9.10 mmol) of the silica precursor 1,2-bis(triethoxysilyl)ethane was added at 40 °C. After a pre-hydrolysis period of 40 min, 0.44 g (0.90 mmol) of 3-(3-sulfopropyl)-1-(3-(triethoxysilyl)propyl)-1*H*-imidazol-3-ium hydrosulfate (**1**) was added. The reaction mixture was stirred at 40 °C for 24 h and then aged at 100 °C for 24 h. The resulting solid was filtered, rinsed with excess ethanol, and then dried overnight on a filter. The surfactant template was removed by refluxing in acidic ethanol (400 mL per gram) for 24 h. The solid was filtered, rinsed with ethanol again, and then dried at 60 °C under reduced pressure overnight to afford HO_3S-PMO (**3**) (1.82 g) in the form of a white powder. IR (KBr) cm^{-1}: 3434.7 (s), 2983.0 (w), 2896.2 (w), 1634.6 (m), 1412.7 (w), 1261.7 (m), 1158.8 (s), 1031.8 (s), 904.9 (m), 808.7 (m), 697.8 (m). Elemental analysis (%): C 15.82, H 1.23, N 0.61, S 1.41. S_{BET}: 740.0 m^2/g, d_{pore}: 8.02 nm, V_{pore}: 0.90 cm^3/g. ^{29}Si MAS NMR (79.4 MHz): T^1 (δ = −49.3 ppm), T^2 (δ = −58.3 ppm), T^3 (δ = −64.7 ppm). ^{13}C CP/MAS NMR (161.9 MHz): 137.4, 124.1 (<u>C</u>H of imidazolium), 56.5 (—O<u>C</u>H_2CH$_3$), 47.3 (—N<u>C</u>H_2CH_2CH_2S—), 37.1 (—N<u>C</u>H_2CH_2CH_2Si—), 21.9 (—OCH$_2$-<u>C</u>H_3), 16.4 (—NCH$_2$<u>C</u>H_2CH_2S—), 8.1–0.5 (—<u>C</u>H_2Si) ppm.

2.2.2. Preparation of the heterogeneous catalyst **5**

In a typical synthesis, Ag_2O (115.5 mg, 0.5 mmol) was added to a suspension of HO_3S-PMO (**3**) (1.00 g) in 20.0 mL of distilled water at room temperature, and the resulting mixture was stirred at 90 °C for 6 h. After cooling to ambient temperature, a solution of 2.0 N H_2SO_4 (10 mL) was added and the mixture was stirred overnight. The solids were collected by centrifugation and washed repeatedly with excess distilled water. The collected light-gray solids were suspended in a solution of 10.0 mL of methanol and 10.0 mL distilled water, and 159.2 mg (0.20 mmol) of $[Cp^*IrCl_2]_2$ was added to the solution at ambient temperature. The resulting mixture was stirred for 12 h. Finally, 176.8 mg (0.40 mmol) of (*S*,*S*)-pentafluorophenylsulfonyl-1,2-diphenylethylenediamine was added and the mixture was stirred further for 6 h at ambient temperature. The mixture was filtered through filter paper and then rinsed with excess water and CH_2Cl_2. After Soxhlet extraction for 24 h in CH_2Cl_2 to remove homogeneous and unreacted starting materials, the solid was dried at ambient temperature under vacuum overnight to afford catalyst **5** (1.13 g) as a light-yellow powder. ICP analysis showed that the Ir loading was 44.16 mg (0.23 mmol) per gram of catalyst and the residual Ag amount was 8.51 mg (0.078 mmol) per gram of catalyst. IR (KBr) cm^{-1}: 3426.7 (s), 2983.0 (w), 2896.1 (w), 1634.6 (m), 1491.6 (w), 1412.8 (w), 1261.7 (m), 1158.8 (s), 1031.8 (s), 912.9 (m), 769.9 (m), 697.8 (m) 441.7 (m). Elemental analysis (%): C 9.07, H 1.66, N 1.29, S 2.21. S_{BET}: 516.4 m^2/g, d_{pore}: 7.85 nm, V_{pore}: 0.72 cm^3/g. ^{29}Si MAS NMR (79.4 MHz): T^1 (δ = −48.3 ppm), T^2 (δ = −58.5 ppm), T^3 (δ = −65.6 ppm). ^{13}C CP/MAS NMR (161.9 MHz): 137.5, 123.7 (<u>C</u>H of imidazolium), 119.5 (<u>C</u>H of Ph), 97.9 (<u>C</u> of Cp ring), 69.8–67.6 (—N<u>C</u>HPh—), 56.5 (—O<u>C</u>H_2-CH$_3$), 47.3 (—N<u>C</u>H_2CH_2<u>C</u>H_2S—), 37.2 (—N<u>C</u>H_2CH_2CH_2Si—), 21.9 (—OCH$_2$<u>C</u>H_3), 16.4 (—NCH$_2$<u>C</u>H_2CH_2S—), 12.3 (Cp<u>C</u>H_3), 8.2–0.5 (—<u>C</u>H_2Si) ppm.

2.2.3. Preparation of the heterogeneous catalyst **6**

6 was prepared according to the general procedure for **5** using (*S*,*S*)-methylsulfonyl-1,2-diphenylethylenediamine instead of 1,2-bis(triethoxysilyl)ethylane-(*S*,*S*)-pentafluorophenylsulfonyl-1,2-diphenylethylenediamine. The solid was dried under reduced pressure overnight to afford catalyst **6** as a light-yellow powder. ICP analysis showed that the Ir loading was 48.35 mg (0.25 mmol) per gram of catalyst and the residual Ag amount was 9.83 mg (0.091 mmol) per gram of catalyst. IR (KBr) cm^{-1}: 3455.1 (s), 2926.1 (w), 2895.9 (w), 1635.1 (m), 1411.4 (w), 1268.7 (m), 1156.9 (s), 1031.7 (s), 919.9 (m), 788.1 (m), 706.3 (m), 452.6 (m). Elemental analysis (%): C 7.71, H 1.72, N 1.40, S 2.41; S_{BET}: 524.2 m^2/g, d_{pore}: 7.92 nm, V_{pore}: 0.75 cm^3/g. ^{29}Si MAS NMR (79.4 MHz): T^1 (δ = −49.4 ppm), T^2 (δ = −58.4 ppm), T^3 (δ = −65.1 ppm). ^{13}C CP/MAS NMR (161.9 MHz): 137.6, 123.9 (<u>C</u>H of imidazolium), 119.2 (<u>C</u>H of Ph), 97.8 (<u>C</u> of Cp ring), 69.9–67.4 (—N<u>C</u>HPh), 56.5 (—O<u>C</u>H_2CH$_3$), 47.3 (—N<u>C</u>H_2CH_2<u>C</u>H_2S—, <u>C</u>H_3SO_2—), 37.3 (—N<u>C</u>H_2CH_2CH_2Si—), 22.0 (—OCH$_2$<u>C</u>H_3), 16.4 (—NCH$_2$<u>C</u>H_2CH_2-S—), 12.2 (Cp<u>C</u>H_3), 8.3–0.5 (—<u>C</u>H_2Si) ppm.

2.3. Catalytic experiments

A typical procedure was as follows. For enantioselective reduction of α-cyanoacetophenones or α-nitroacetophenones, catalyst **5** (8.70 mg, 2.0 μmol of Ir, based on ICP analysis), acetophenones (0.80 mmol), and an aqueous solution of formic acid (5.0 equiv.

1.0 M formate solution, 0.2 M overall concentration, for X = CN, pH = 3.5; for X = NO_2, pH = 2.0) were added sequentially to a 10.0 mL round–bottom flask. The mixture was then stirred at room temperature (25 °C) for 5–20 h. [*For enantioselective reduction of β-ketoesters*, catalyst **6** (8.0 mg, 2.0 μmol of Ir, based on ICP analysis), β-ketoesters (0.80 mmol), and an aqueous sodium formate solution (5.0 equiv. 1.0 M formate solution, 0.2 M overall concentration, pH = 8.0) were added to a 10.0 mL roundbottom flask in turn. The mixture was then stirred at 4 °C for 6–8 h.] During this period, the reaction was monitored constantly by TLC. After the completion of the reaction, the catalyst was separated by centrifugation (10,000 rpm) for the recycling experiment. The aqueous solution was extracted with ethyl ether (3 × 3.0 mL). The combined ethyl ether extracts were washed with brine twice and then dehydrated with Na_2SO_4. After evaporation of ethyl ether, the residue was purified by silica gel flash column chromatography to afford the desired product. The conversion was calculated through the external standard method, and the ee value was determined by a HPLC analysis using a UV–Vis detector and a Daicel OJ-H chiralcel column (Φ 0.46 × 25 cm).

3. Results and discussions

3.1. Synthesis and characterization of catalyst 5

Imidazolium-based, chiral Cp*IrPFPSDPEN-functionalized periodic mesoporous organosilica, abbreviated as Cp*IrPFPSDPEN-PMO (**5**), (Cp*IrPFPSDPEN: [25–27] Cp* = pentamethylcyclopentadiene, PFPSDPEN = (*S*,*S*)-pentafluorophenylsulfonyl-1,2-diphenylethylenediamine (**4**)) was prepared as outlined in Scheme 1. First, 3-(3-sulfopropyl)-1-(3-(triethoxysilyl)propyl)-1*H*-imidazol-3-ium hydrosulfate (**1**) was obtained through the reaction of 1-(3-(triethoxysilyl)propyl)-1*H*-imidazole and 1,3-propane-sultone according to a reported method [28]. Co-condensation of **1** and 1,2-bis(triethoxysilyl)ethylane (**2**) using P123 as a structure-directing template afforded HO_3S-PMO (**3**) as a white powder. Finally, the continuous ion exchanges with Ag_2O [29] and $(Cp^*IrCl_2)_2$ followed by complexation of (**4**) [30] led to the crude heterogeneous catalyst **5** in which the potential formation of imidazolyl-Ag or imidazolyl-Ir complexes had not been observed [29,31]. This was subjected to Soxhlet extraction to clear its nanochannels and to obtain its pure form, which was a light-yellow powder.

Fig. 1 shows the FT-IR spectra of the HO_3S-PMO (**3**) and catalyst **5**. Generally, both **3** and **5** exhibited the characteristic bands of the PMO-type materials around 3430, 1635 and 1031 cm^{-1} for υ(O—H), δ(O—H) and υ(Si—O), respectively [32]. The relatively

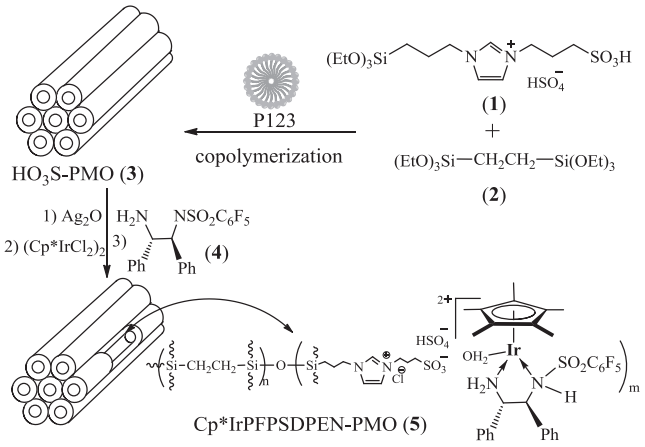

Scheme 1. Preparation of the heterogeneous catalyst **5**.

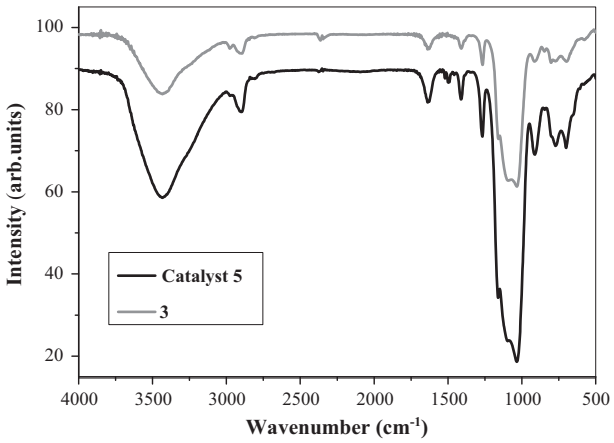

Fig. 1. FT-IR spectra of HO_3S-PMO (**3**) and catalyst **5**.

weak bands between 3100–2800 cm^{-1} were assigned to asymmetric and symmetric stretching vibrations of C—H bonds. The peaks indicative of υ(Si—C) should appear at 1100 cm^{-1}, however, they were difficult to be distinguished because of the overlapping by the absorbance from υ(Si—O) [33]. The bands between 1610–1450 cm^{-1} were attributed to breathing vibrations of C=C bonds in the aromatic ring [32]. These peaks increased consistently in catalyst **5** relatively to that in the spectrum of **3**, implying that (*S*,*S*)-pentafluorophenylsulfonyl-1,2-diphenylethylenediamine (**4**) participated in the coordination of Ir centers. All these observations demonstrated the successful incorporation of chiral Cp*IrPFPSDPEN complexes within the periodic mesoporous organosilica.

Incorporation of well-defined single-site active iridium centers within the organosilicate network of **5** could be proven by solid-state ^{13}C cross-polarization (CP)/magic angle spinning (MAS) NMR spectroscopy. As shown in Fig. 2, both **3** and **5** produced strong, characteristic carbon signals of $Si\underline{C}H_2\underline{C}H_2Si$ groups at ~5 ppm, corresponding to ethylene-bridged organosilica embedded within their organosilicate networks. Carbon atoms of N$\underline{C}$H groups of the TsDPEN moiety could be observed clearly at ~68 ppm in their spectra. Peaks at ~98 and ~12 ppm in the spec-

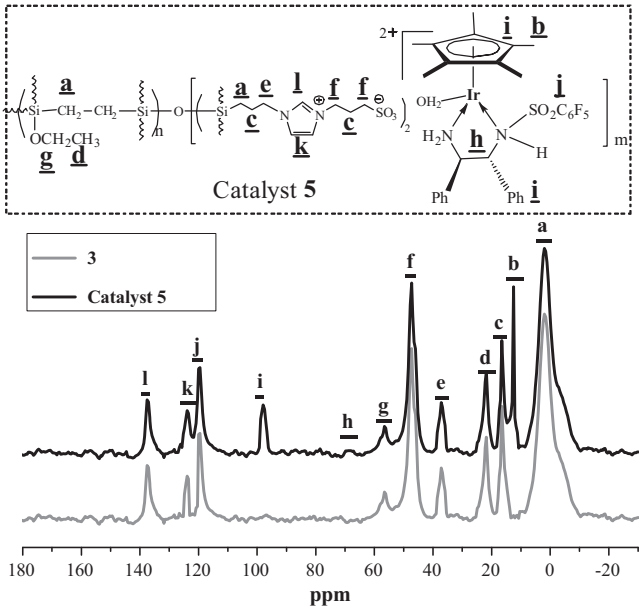

Fig. 2. ^{13}C CP MAS NMR spectra of HO_3S-PMO (**3**) and catalyst **5**.

trum of **5** are ascribed to the carbon atoms of the Cp ring and to the carbon atoms of the $\underline{C}H_3$ groups attached to Cp, respectively. These peaks are absent in the spectrum of **3**, suggesting the formation of the Cp*IrPFPSDPEN complex. Chemical shifts of **5** were similar to those of its homogeneous counterpart (Cp*IrPFPSDPEN) [25], demonstrating that they had the same well-defined single-site active species. In addition, carbon signals of imidazolium and of propyl moiety could also be observed (marked in the spectra). Peaks at ~22 and ~57 ppm typically present in the ^{13}C CP/MAS spectra are attributed to the unhydrolyzed ethoxy groups (—O$\underline{C}H_2\underline{C}H_3$) [34].

The organosilicate network and the composition of Cp*IrPFPSDPEN active centers in **5** could be confirmed by solid-state ^{29}Si MAS NMR spectroscopy. As shown in Fig. 3, both **3** and **5** produced one group of exclusive T signals derived from organosilica, suggesting that all Si species were covalently attached to carbon atoms [6]. Typical isomer shift values of **5** were similar to values reported in the literature [35] (−48.5, −58.5, and −67.5 ppm for T^1, T^2, and T^3 of [$R(HO)_2SiOSi$], [$R(HO)Si(OSi)_2$], and [$RSi(OSi)_3$], respectively). Notably, strong T signals at −58 and −65 ppm in the spectrum of **5** are attributed to T^2(R–Si$(OSi)_2$(OH)] and T^3(R–Si$(OSi)_3$), respectively (R = Cp*IrPFPSDPEN functionalities or ethylene-bridged groups). These observations demonstrate that both **3** and **5** possessed organosilicate networks with R-Si$(OSi)_2$(OH) and R-Si$(OSi)_3$ species in their main organosilicate networks. Furthermore, the absence of signals for Q-series from −90 to −120 ppm indicates that the carbon–silicon bond was not cleaved during the hydrolysis–condensation process.

To investigate the electronic state of the iridium center, X-ray photoelectron spectroscopy (XPS) of **5** and its homogeneous Cp*-IrPFPSDPEN was carried out. As shown in Fig. 4, **5** had Ir $4f_{7/2}$ binding energy similar to that of Cp*IrPFPSDPEN (62.48 eV vs 62.46 eV), but both Ir $4f_{7/2}$ binding energies were obviously different from that of their parent $(Cp^*IrCl_2)_2$ complex (61.81 eV) (see SI in Fig. S1). This difference indicates the formation of single-site Cp*-IrPFPSDPEN active centers within the organosilicate network of **5**. These results are verified by ^{13}C CP/MAS NMR spectra. The active centers play a key role in the enantioselective performance, as discussed in the next section.

The ordered mesostructure and well-defined pore arrangement of **5** were further investigated by using X-ray diffraction (XRD), transmission electron microscopy (TEM), and nitrogen adsorption–desorption measurements. The small-angle XRD patterns (Fig. 5) reveal that both **3** and **5** produced an intense d_{100} diffraction peak along with two similar weak diffraction peaks (d_{110}, d_{200}), suggesting that the dimensional-hexagonal pore structure (*p6mm*) observed in general PMO materials could be preserved after co-condensation [18,19]. The TEM images (Fig. 6) further confirm that **5** had a highly ordered mesostructure with dimensional-hexagonal arrangements, in which the SEM image with a chemical mapping of **5** had the uniform distribution of Ir (see SI in Fig. S2). The nitrogen adsorption–desorption isotherm of **5** (Fig. 7) is a typical type IV isotherm with an H_1 hysteresis loop and a visible step at P/P_0 = 0.50–0.90, corresponding to capillary condensation of nitrogen in mesopores. Structural parameters of **3** and **5** are listed in a table inset in Fig. 5.

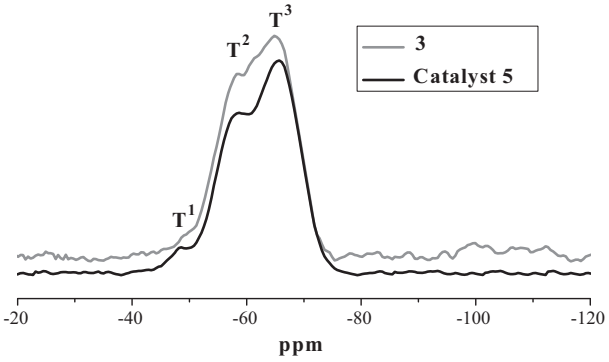

Fig. 3. ^{29}Si CP MAS NMR spectra of HO_3S-PMO (**3**) and catalyst **5**.

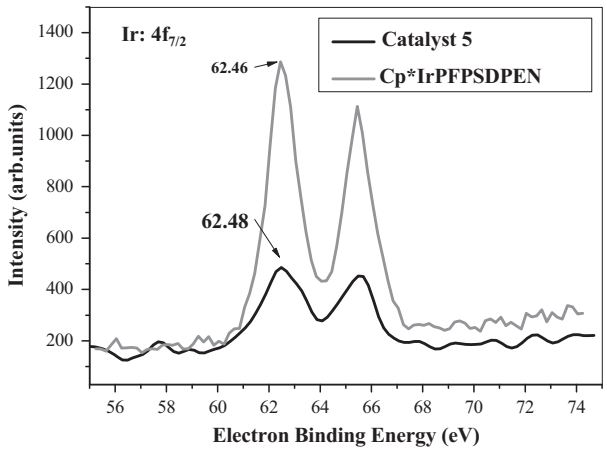

Fig. 4. XPS spectra of Cp*IrPFPSDPEN and catalyst **5**.

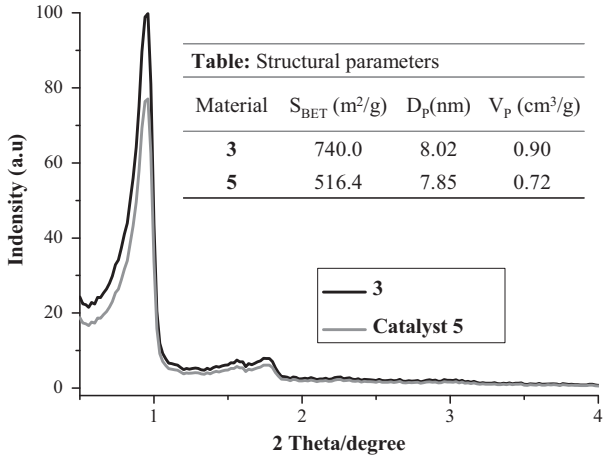

Fig. 5. Small-angle powder XRD patterns of HO_3S-PMO (**3**) and catalyst **5**.

Above characterizations and analyses suggest that the imidazolium-based, chiral organoiridium-functionalized PMO containing well-defined single-site Cp*IrPFPSDPEN active species within its ordered dimensional-hexagonal nanostructure could be readily constructed through the co-condensation strategy.

3.2. Catalytic property of the heterogeneous catalyst **5**

3.2.1. Catalytic performance

The chiral N-sulfonylated diamine-based organometallic complexes, a type of highly enantioselective catalysts, have been used extensively in various studies on asymmetric transfer hydrogenation [25–27,36]. In the present study, we first examined its catalytic activity and enantioselectivity in the reduction of α-cyanoacetophenone in aqueous medium. Reaction with the hydrogen source HCO_2H and 0.25% mol PMO as a catalyst was investigated according to a reported method [25]. Enantioselective reduction of benzoylacetonitrile catalyzed by **5** gave (*S*)-3-hydroxy-3-phenylpropanenitrile with >99% conversion and 97%

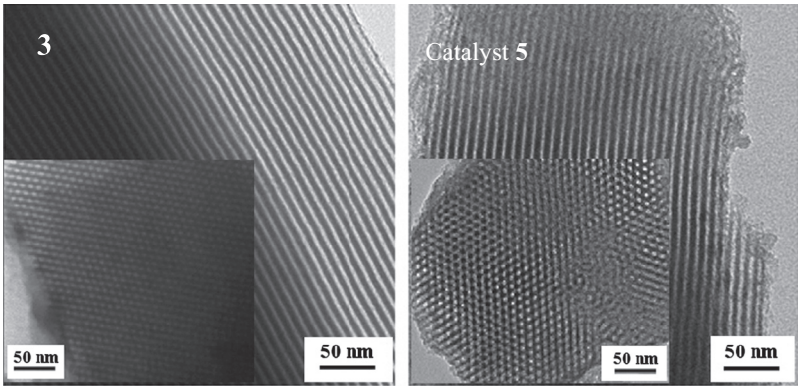

Fig. 6. TEM images of HO_3S-PMO (**3**) and catalyst **5** viewed along [100] and [001] directions.

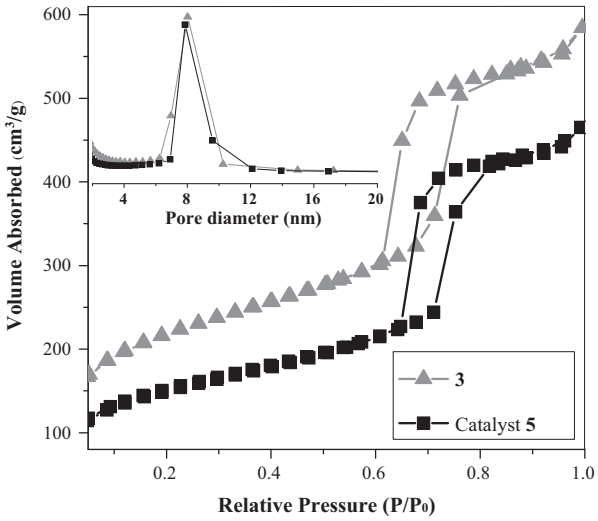

Fig. 7. Nitrogen adsorption–desorption isotherms of HO_3S-PMO (**3**) and catalyst **5**.

ee value. Such an ee value seems to be a small increase relative to that of Cp*IrPFPSDPEN (entry 1 vs entry 1 in brackets, Table 1). In addition, the asymmetric reaction could be run at much higher substrate-to-catalyst mole ratio without apparently affecting its ee value, as exemplified by the enantioselective reduction of benzoylacetonitrile at substrate-to-catalyst mole ratio of 600 (entry 2, Table 1).

Because of its high catalytic performance, **5** was further investigated by using it in the enantioselective reductions of α-cyanoacetophenones with various substituents on the Ar moiety. As shown in Table 1, high conversions, no side products, and high enantioselectivities were obtained for all tested substrates under the same reaction conditions. The electronic properties of substituents at the Ar moiety of acetophenones did not affect enantioselectivities, that is, various electron-withdrawing and -donating substituents of the Ar moiety led to the same efficiency (entries 4–9). The enantioselective reduction was also suitable for the asymmetric transfer hydrogenation of α-nitroacetophenones. Similarly, high conversions, no side products, and high enantioselectivities could also be obtained for a series of α-nitro-substituted acetophenones (entries 10–15).

3.2.2. Investigation of factors affecting catalytic performance

It is noteworthy that the asymmetric reactions catalyzed by **5** have rates higher than that attained with a previously reported inorganosilica-supported Cp*IrPFPSDPEN-functionalized heterogeneous catalyst [22], and even markedly higher than that attained with Cp*IrPFPSDPEN [25]. For example, we found that the enantioselective reduction of benzoylacetonitrile catalyzed by **5** could be completed within 5 h, whereas the reaction catalyzed by its inorganosilicate analog and by Cp*IrPFPSDPEN required 12 h [22] and 24 h, respectively. The drastically enhanced reaction rates attained with **5** are due to the potential imidazolium-functionality and high hydrophobicity of ethylene-bridged PMO. To confirm this judgment, the kinetic profile of the enantioselective reduction of benzoylacetonitrile catalyzed by **5**, by its inorganosilicate analog, and by Cp*IrPFPSDPEN were investigated. The initial activity of **5** was evidently higher than that of its inorganosilicate analog, and even higher than that of Cp*IrPFPSDPEN; the initial TOF values were 122.0, 60.0 and 39.0 mol/(mol h), respectively (Fig. 8). Notably, the reaction rate with **5** was twice that with its inorganosilicate-supported analog and thrice that with Cp*IrPFPSDPEN. These results suggest that the enhanced rate of asymmetric organic

Table 1
Enantioselective reduction of α-cyano and α-nitroacetophenones.[a]

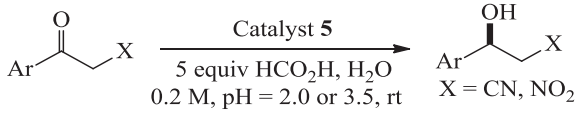

Entry	Ar, X	Time (h)	Conv. (%)[b]	Ee (%)[b]
1	Ph, CN	5 (24)	>99 (99)	97 (94)[c]
2	Ph, CN	20	93	96[d]
3	Ph, CN	5	95	94[e]
4	4-FPh, CN	5	>99	96
5	3-ClPh, CN	5	>99	94
6	4-MePh, CN	5	>99	96
7	3-MeOPh, CN	5	>99	95
8	2-furyl, CN	10	>99	98
9	2-thiophenyl, CN	10	>99	97
10	Ph, NO_2	5	>99	98
11	4-FPh, NO_2	5	>99	95
12	4-ClPh, NO_2	5	>99	94
13	2-ClPh, NO_2	5	>99	92
14	4-MePh, NO_2	5	>99	97
15	4-MeOPh, NO_2	5	>99	95

[a] Reaction conditions: catalyst **5** (8.70 mg, 2.0 μmol of Ir based on the ICP analysis), α-cyanoacetophenones (α-nitroacetophenones) (0.80 mmol) and the aqueous solution of formic acid (5.0 equiv, 1.0 M formate solution, 0.2 M overall concentration, for X = CN, pH = 3.5; for X = NO_2, pH = 2.0), reaction temperature (25 °C) and reaction time (5–20 h).
[b] Determined by chiral HPLC analysis (see SI in Figs. S3 and S7).
[c] Data in the bracket were obtained using the homogenous Cp*IrPFPSDPEN as a catalyst reported in the literature [7].
[d] Data were obtained using catalyst **5** at substrate-to-catalyst mole ratio of 600.
[e] Data were obtained using the mixed HO_3S-PMO (**3**) plus its homogeneous Cp*IrPFPSDPEN as a catalyst.

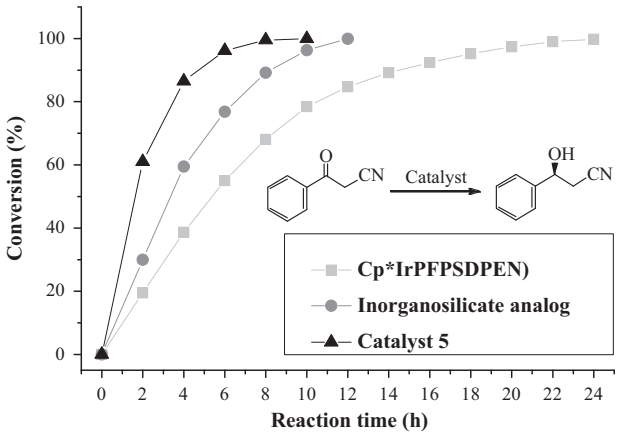

Fig. 8. Comparison of the asymmetric transfer hydrogenations of benzoylacetonitrile catalyzed by **5**, by its inorganosilicate analog, and by its homogeneous Cp*IrPFPSDPEN. Reactions were carried out at substrate-to-catalyst mole ratio of 400.

transformation by **5** is due to the combination of the imidazolium-functionality and the high hydrophobicity of ethylene-bridged organosilicate.

Interestingly, asymmetric reactions catalyzed by **5** seem to be a small increase in enantioselectivity for most tested substrates, relative to those with its homogeneous Cp*IrPFPSDPEN [25]. For example, enantioselective reduction of benzoylacetonitrile catalyzed by **5** gave 97% ee of the target products, which is higher than 94% ee obtained with its homogeneous Cp*IrPFPSDPEN. This difference indicates that the incorporation of chiral Cp*IrPFPSDPEN functionality within the imidazolium-based PMO could result in slightly enhanced enantioselectivity. To obtain deeper insight into the effect, a parallel enantioselective reduction of benzoylacetonitrile catalyzed by a mixture of **3** plus its homogeneous Cp*IrPFPSDPEN was investigated. The result shows that the asymmetric reaction gave (*S*)-3-hydroxy-3-phenylpropanenitrile with 95% conversion and 94% ee (entry 3, Table 1). The same ee value as that obtained with Cp*IrPFPSDPEN reveals that the reaction catalyzed by the catalyst mixture retained its original, homogenous enantioselectivity [22]. However, the ee value is low relative to that obtained with **5** (94% ee vs 97% ee), suggesting that the enhanced ee value with **5** was originated from the imidazolium-based chiral Cp*IrPFPSDPEN-PMO material itself. Indirect evidence supporting this hypothesis came from an XPS investigation discussed above, in which both the similar Ir $4f_{7/2}$ binding energy indicates that the active iridium center in **5** had the same coordinated environment as that of Cp*IrPFPSDPEN. Thus, the enhanced enantioselectivity could be ascribed to the well-defined single-site active iridium species with the ethylene-bridged organosilicate network proved by above ^{13}C NMR.

3.2.3. Catalyst recycling and reuse

Another important consideration in the design of a heterogeneous catalyst is the ease of separation by simple centrifugation and the ability of the catalyst to retain its catalytic activity and enantioselectivity after multiple cycles of use. As shown in Table 2, the heterogeneous catalyst **5** was recovered easily and reused repeatedly in eight consecutive reactions for enantioselective reduction of benzoylacetonitrile as a model reaction. At eighth recycle, catalyst **5** still afforded 99.0% conversion and 94.5% ee (see SI in Fig. S4). ICP analysis showed that the amount of Ir at 8th cycle was 42.30 mg per gram of catalyst and only 4.2% of the Ir content was lost. This result should be ascribed the fact that the uniformly distributed counterions associated with the imidazolium and sulfonates within the wall of nanopores could avoid efficiently the leaching of Ir, thereby resulting in a high recyclability.

3.2.4. Expansion of enantioselective reduction

Furthermore, as an approach of direct postcoordination of chiral ligands, the immobilized strategy could also be used to easily construct other heterogeneous catalysts. As shown in Scheme 2, a similar imidazolium-based chiral Cp*IrMsDPEN-functionalized PMO (Cp*IrMsDPEN: [37,38] MsDPEN = methylsulfonyl-1,2-diphenylethylenediamine), denoted as Cp*IrMsDPEN-PMO (**6**), could be readily constructed by substitution of (*S*,*S*)-PFPSDPEN with (*S*,*S*)-

Table 2
Reusability of catalysts **5**–**6** for asymmetric reactions.

Catalyst	Run time	1	2	3	4	5	6	7	8	9
5	% Conv.[a]	>99.9	99.5	99.5	99.5	99.3	99.3	99.1	99.0	88.2
	% ee[a]	97.1	96.1	95.8	94.4	94.8	94.8	94.6	94.5	94.4
6	% Conv.[b]	>99.9	99.7	99.5	99.4	99.4	99.3	99.3	99.1	87.6
	% ee[b]	97.2	97.2	97.1	96.8	96.4	96.4	96.3	96.0	94.8

[a] Reaction conditions: Catalyst **5** (87.0 mg, 20.0 μmol of Ir based on the ICP analysis), benzoylacetonitrile (8.0 mmol), the aqueous solution of formic acid (5.0 equiv, 1.0 M formate solution, 0.2 M overall concentration, pH = 3.5), reaction temperature (25 °C), reaction time (5 h).
[b] Reaction conditions: catalyst **6** (80.0 mg, 20.0 μmol of Ir based on the ICP analysis), ethyl benzoylacetate (8.0 mmol), aqueous sodium formate solution (5.0 equiv. 1.0 M formate solution, 0.2 M overall concentration, pH = 8.0), reaction temperature (4 °C) and reaction time (6 h).

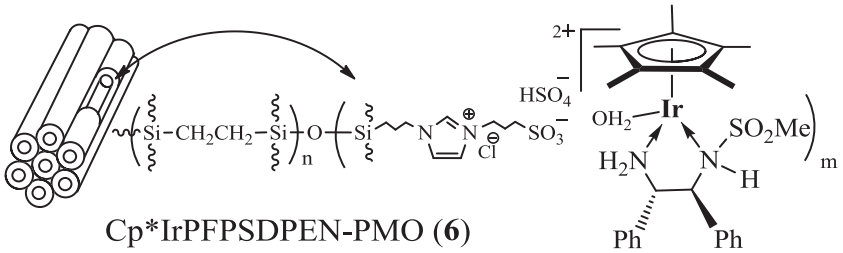

Scheme 2. Structure of the heterogeneous catalyst **6**.

Table 3
Enantioselective reduction of β-ketoesters.[a]

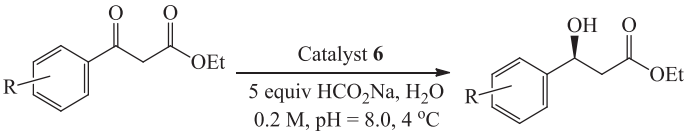

Entry	R	Time (h)	Conv. (%)[b]	Ee (%)[b]
1	H	6 (24)	>99 (96)	97 (96)
2	4-F	6	>99	95
3	3-Cl	6	>99	94
4	2-Cl	6	>99	60
5	4-Br	6	>99	98
6	4-I	6	>99	94
7	4-Me	6	>99	97
8	4-OMe	6	>99	97
9	4-NO_2	6	>99	95
10	4-CF_3	6	>99	96
11	2-furyl	8	>99	97

[a] Reaction conditions: catalyst **6** (8.0 mg, 2.0 μmol of Ir based on the ICP analysis), β-ketoesters (0.80 mmol) and the aqueous sodium formate solution (5.0 equiv. 1.0 M formate solution, 0.2 M overall concentration, pH = 8.0), reaction temperature (4 °C), reaction time (6–8 h).
[b] Determined by chiral HPLC analysis (see SI in Figs. S5 and S7).

MsDPEN through the same procedure. As shown in Table 3, **6** also displayed high catalytic activity and high enantioselectivity in the reduction of β-ketoesters in aqueous medium. Similarly, enhanced reaction ratio and enantioselectivity could be obtained in this case. As expected, the heterogeneous catalyst **6** could also be recovered easily and reused repeatedly in the enantioselective reduction of ethyl benzoylacetate as a model reaction (Table 2). The recycling catalyst **6** still afforded 99.1% conversion and 96.0% ee at eighth recycle (see SI in Fig. S6). This result suggests that the immobilizated strategy described here could be a potential way for anchoring various chiral ligands to construct imidazolium-based, chiral organometal-functionalized periodic mesoporous organosilica.

4. Conclusions

In conclusions, using a co-condensation method, we incorporated the imidazolium functionality within an ethylene-bridged PMO. Utilizing a direct postcoordination of chiral ligands, we developed two chiral organoiridium-functionalized heterogeneous catalysts. The chiral PFPSDPEN-based heterogeneous catalyst **5** displayed catalytic activity and enantioselectivity higher than those of its homogeneous counterpart Cp*IrPFPSDPEN in the enantioselective reduction of α-cyanoacetophenones and α-nitroacetophenones in aqueous medium. As presented in this study, the imidazolium-functionality and the hydrophobic PMO could enhance the catalytic performance in aqueous asymmetric reactions. In addition, the heterogeneous catalyst **5** could be recovered and reused for at least eight times without loss of its catalytic activity. The immobilization approach could be used to easily construct another chiral, methylsulfonyl-1,2-diphenylethylenediamine-based organoiridium-functionalized-PMO (**6**) and to realize highly efficient enantioselective reduction of β-ketoesters in aqueous medium.

Acknowledgments

We are grateful to Shanghai Sciences and Technologies Development Fund (12nm0500500 and 13ZR1458700), CSIRT (IRT1269) and Shanghai Municipal Education Commission (12ZZ135, 14YZ074 and SK201329) for financial supports.

Appendix A. Supplementary material

Experimental procedure and analytical data for obtained chiral products. This material is available free of charge *via* editor office. Supplementary data associated with this article can be found, in the online version, at http://dx.doi.org/10.1016/j.jcat.2014.09.019.

References

[1] N. Mizoshita, T. Taniab, S. Inagaki, Chem. Soc. Rev. 40 (2011) 789.
[2] F. Hoffmann, M. Fröba, Chem. Soc. Rev. 40 (2011) 608.
[3] F. Kleitz, Handbook of Asymmetric Heterogeneous Catalysis, Wiley-VCH, Weinheim, 2008. pp. 178.
[4] C.E. Song, in: K.L. Ding, Y. Uozumi (Eds.), Handbook of Asymmetric Heterogeneous Catalysis, Wiley-VCH, Weinheim, 2009, p. 25.
[5] M.E. Davis, Nature 417 (2002) 813.
[6] S. Inagaki, S. Guan, T. Ohsuna, O. Terasaki, Nature 416 (2002) 304.
[7] J. Dupont, R.F. de Souza, P.A.Z. Suarez, Chem. Rev. 102 (2002) 3667.
[8] B. Karimi, M. Gholinejad, M. Khorasani, Chem. Commun. 48 (2012) 8961.
[9] B. Karimi, D. Elhamifar, O. Yari, M. Khorasani, H. Vali, J.H. Clark, A.J. Hunt, Chem. Eur. J. 18 (2012) 13520.
[10] P. Borah, X. Ma, K.T. Nguyen, Y. Zhao, Angew. Chem. Int. Ed. 51 (2012) 7756.
[11] M. Waki, N. Mizoshita, T. Tani, S. Inagaki, Angew. Chem. Int. Ed. 50 (2011) 11667.
[12] M. Guan, W. Wang, E.J. Henderson, Ö. Dag, C. Kübel, V.S.K. Chakravadhanula, J. Rinck, I.L. Moudrakovski, J. Thomson, J. McDowell, A.K. Powell, H. Zhang, G.A. Ozin, J. Am. Chem. Soc. 134 (2012) 8439.
[13] M. Mandal, Mi. Kruk, Chem. Mater. 24 (2012) 123.
[14] A. Kuschel, S. Polarz, J. Am. Chem. Soc. 132 (2010) 6558.
[15] X. Wu, T. Blackburn, J.D. Webb, A.E. Garcia-Bennett, C.M. Crudden, Angew. Chem. Int. Ed. 50 (2011) 8095.
[16] X. Liu, P.Y. Wang, L. Zhang, J. Yang, C. Li, Q.H. Yang, Chem. Eur. J. 16 (2010) 12727.
[17] R.A. Garcia, R. van Grieken, J. Iglesias, V. Morales, N. Villajos, J. Catal. 274 (2010) 221.
[18] K. Liu, R. Jin, T. Cheng, X. Xu, F. Gao, G. Liu, H. Li, Chem. Eur. J. 18 (2012) 15546.
[19] R. Liu, R. Jin, L. Kong, J. Wang, C. Chen, T. Cheng, G. Liu, Chem. Asian. J. 8 (2013) 3108.
[20] W. Xiao, R. Jin, T. Cheng, D. Xia, H. Yao, F. Gao, B. Deng, G. Liu, Chem. Commun. 48 (2012) 11898.
[21] D. Xia, T. Cheng, W. Xiao, K. Liu, Z. Wang, G. Liu, H. Li, W. Wang, ChemCatChem 5 (2013) 1784.
[22] B. Deng, T. Cheng, M. Wu, J. Wang, G. Liu, ChemCatChem 5 (2013) 2856.
[23] J. Long, G. Liu, T. Cheng, H. Yao, Q. Qian, J. Zhuang, F. Gao, H. Li, J. Catal. 298 (2013) 41.
[24] R. Liu, T. Cheng, L. Kong, C. Chen, G. Liu, H. Li, J. Catal. 307 (2013) 55.
[25] O. Soltani, M.A. Ariger, H. Vázquez-Villa, E.M. Carreira, Org. Lett. 12 (2010) 2893.
[26] H. Vázquez-Villa, S. Reber, M.A. Ariger, E.M. Carreira, Angew. Chem. Int. Ed. 50 (2011) 8979.
[27] R. ter Halle, E. Schulz, M. Lemaire, Synlett (1997) 1257.
[28] J.M. Miao, H. Wan, Y.B. Shao, G.F. Guan, B. Xu, J. Mol. Catal. A: Chem. 348 (2011) 77.
[29] S. Hiraoka, M. Shiro, M. Shionoya, J. Am. Chem. Soc. 126 (2004) 1214.
[30] S. Ogo, N. Makihara, Y. Watanabe, Organometallics 18 (1999) 5470.
[31] T.K. Maishal, J. Alauzun, J. Basset, C. Copéret, R.J.P. Corriu, E. Jeanneau, A. Mehdi, C. Reyé, L. Veyre, C. Thieuleux, Angew. Chem. Int. Ed. 47 (2008) 8654.
[32] A.S.M. Chong, X.S. Zhao, J. Phys. Chem. B 107 (2003) 12650.
[33] H. Huang, R. Yang, D. Chinn, C.J. Munson, Ind. Eng. Chem. Res. 42 (2003) 2427.
[34] P.F.W. Simon, R. Ulrich, H.W. Spiess, U. Wiesner, Chem. Mater. 13 (2001) 3464.
[35] O. Krőcher, O.A. Kőppel, M. Fröba, A. Baiker, J. Catal. 178 (1998) 284.
[36] R. Malacea, R. Poli, E. Manoury, Coordin. Chem. Rev. 254 (2010) 729.
[37] M.A. Ariger, E.M. Carreira, Org. Lett. 14 (2012) 4522.
[38] J.H. Xie, X.Y. Liu, X.H. Yang, J.B. Xie, L.X. Wang, Q.L. Zhou, Angew. Chem. Int. Ed. 51 (2012) 201.